

Structural and shielding properties of the tellurite-tungsten glass matrix with addition zinc fluoride

A. Z. Alzuhair^a, M. S. Alqahtani^{a,b}, A. J. Alkulib^{a,g,*}, K. I. Hussein^{a,e}, M. Reben^f, E. Yousef^{c,d}

^aDepartment of Radiological Sciences, College of Applied Medical Sciences, King Khalid University, Abha 61421, Saudi Arabia

^bBioImaging Unit, Space Research Centre, Department of Physics and Astronomy, University of Leicester, Leicester LE1 7RH, UK

^cPhysics Department, Faculty of Science, King Khalid University, Postcode: 9004, Zip code: 61413, Abha, Saudi Arabia

^dResearch Center for Advanced Materials Science (RCAMS), King Khalid University, Postcode: 9004, Zip code: 61413, Abha, Saudi Arabia

^eDepartment of Medical Physics and Instrumentation, National Cancer Institute, University of Gezira, Wad Medani 20, Sudan

^fFaculty of Materials Science and Ceramics, AGH – University of Science and Technology, al. Mickiewicza 30, 30-059 Cracow, Poland

^gMedical Imaging Department, King Faisal Medical City, Abha 61431, Saudi Arabia.

In this study, we reported the radiation protection characteristics of TeO₂-WO₃-ZnF₂ glass systems with different compositions. The composition of the glasses are (0.8 - x) TeO₂-0.2WO₃-xZnF₂, 0.7TeO₂-0.1WO₃-0.2-ZnF₂ and 0.6TeO₂-0.15WO₃-0.25ZnF₂ (where x = 0.1,0.2,0.3). The radiation shielding parameters including mass attenuation coefficient (MAC), linear attenuation coefficient (LAC), half value layer (HVL), mean free path (MFP), tenth value layer (TVL), effective atomic number (Z_{eff}), effective electron number (N_{eff}), and atomic and electronic cross sections (ACS and ECS) have been determined for the prepared glasses against a broad range of ionizing energy between 0.015 and 15 MeV. The structure of the prepared glasses was investigated by using Raman spectra. It obtained that, the incorporation of WO₃ into the TeO₂ glass network causes the creation of W-O-W connections, while Te-O-W linkages with greater electronic polarizability improve the glass network's connectedness. The study demonstrates that the TeO₂-WO₃-ZnF₂ glass system can be utilized for radiation protection against ionizing radiation in a variety of medical and technical applications.

(Received December 28, 2021; Accepted March 10, 2022)

Keywords: Raman spectra, Tungsten tellurite units, Mass attenuation, Shielding material, Cross section, Mean free path

1. Introduction

For the aim of radiation protection, specifically, ionizing radiation and its effect on the human being much research has been utilized during the last decade [1-3]. Ionizing radiation, which includes gamma and x-rays, alpha, beta, neutrons, and higher ultraviolet portion are types of electromagnetic radiation that have sufficient energy to remove an electron from the atom [4, 5]. Diagnostic and therapeutic radiology, nuclear medicine, and other disciplines rely heavily on the use of gamma and x-ray technology. [6]. Radiation protection has grown in importance as a research topic after a better understanding of the potentially harmful effect of ionizing radiation on living tissues [7-9]. Lead (Pb) or lead glasses and concrete are the most traditionally used shielding materials in ionizing radiation facilities and have been examined and analyzed over a broad

* Corresponding author: aalkulib@kfmcity.med.sa
<https://doi.org/10.15251/CL.2022.193.187>

spectrum of ionizing radiation energies [10, 11]. However, lead has many disadvantages compared to other new shielding materials including the cost, toxicity, low melting point, and non-transparency [12]. These limitations have encouraged the researchers to look for superior materials including glass, polymers, ceramics, and alloys that are cost-effective, non-toxic, high density, and have minimal transparency [13-15]. Recently, glass has been attracted researchers as a result of its superior material properties like optical transparency, low cost, and easy manufacturing [6]. Additive oxide-based glasses have promising shielding properties and have already been demonstrated [16, 17]. Furthermore, most of these oxide glasses are cost-effective, have low glass transition, high thermal stability, low melting point, and low crystallization ability [18]. Compared to conventional glasses, heavy-metal-oxide (HMO) based glasses like lead, tellurite, tungsten, and bismuth have superior shielding characteristics for ionizing radiation due to their high electrical conductivity, high rare-earth ion solubility, suitable infrared transmissivity, high optical bandwidth, and low glass transition and melting point [19]. Tellurium oxide (TeO_2) is a type of oxide glass formation that has been considered for use in non-linear optical devices and fiber amplifiers [20]. TeO_2 (Te ($Z=52$))- rich glass (structural units: TeO_4 (trigonal bipyramids), TeO_3 (trigonal pyramids), and $\text{TeO}_{3+\delta}$ polyhedron) has a low melting temperature (< 850 °C), low photon energy (~ 750 cm^{-1}), high dielectric constant, high linear and non-linear refractive index, high optical transmission window ($\sim 0.4\text{-}6$ μm), and fascinating physical properties between other oxide glasses [20-22]. TeO_2 requires the addition of other component material to convert it to a glass structure and this is because of the weak Te-O bonds which give them a distinctive feature, and this can be a beneficial opportunity to add heavy metal oxides and rare earth ions [22, 23]. Tungsten oxide (WO_3) is a non-classical glasses which can possess six multiple states: 0, +2, +3, +4, +5, and +6 [24]. WO_3 is a semiconductor oxide with a small bandgap around 2.8 eV and has been used in gas sensors and solid-state micro-batteries [25]. WO_3 has strong W-O bonds and high polarization ability, which makes it an interesting material in glass technology [26]. Generally, WO_3 is incorporated into telluride, borate, and phosphate glasses to enhance their mechanical and shielding characteristics [26-29]. However, the most popular study is the telluride glass systems including binary TeO_2 - WO_3 glasses [29, 30]. The addition of oxyfluoride glasses has attracted a lot of interest as well as oxide glasses [31]. Oxyfluoride glasses have outstanding optical characteristics such as high refractive index low dispersions, ultraviolet and infrared transmittance, and good chemical and thermal stabilities [32, 33]. Adding ZnF_2 on glass can decrease the glass photon energy and OH group concentration because the ZnF_2 content will react with H_2O and form ZnO and 2 HF which reduce the OH^- vibration in the tellurite glass system, and thus increases the light efficiency [34-37]. Also, increasing the ZnF_2 content in the tellurite glass system can increase the thermal stability, decrease the glass transition temperature (T_g) and the rigidity of glasses, and facilitate crystallization [38]. In this present research, the radiation shielding characteristics of TeO_2 - WO_3 - ZnF_2 glass systems have been studied. For TeO_2 - WO_3 - ZnF_2 glass systems, mass attenuation coefficient (MAC), linear attenuation coefficient (LAC), half-value layer (HVL), mean free path (MFP), tenth value layer (TVL), effective atomic number (Z_{eff}), effective electron number (N_{eff}), and atomic and electronic cross-sections (ACS and ECS) were calculated within photon energy range from 0.015 to 15 MeV using MIKEsoftware [39].

2. Experimental work

2.1. Glass preparation

Glasses with the composition of $(0.8 - x) \text{TeO}_2$ - 0.2WO_3 - $x\text{ZnF}_2$, (where $x = 0.1, 0.2, 0.3$), 0.7TeO_2 - 0.1WO_3 - 0.2-ZnF_2 and 0.6TeO_2 - 0.15WO_3 - 0.25ZnF_2 in mol% made by combining specific raw material weights. The powder mixture was given in a Pt crucible and heated in a melting furnace at temperatures in the range of 750-850 °C for 30 min. The melt was cooled to 700 °C and cast in a graphite mold. Subsequently, the sample was transferred to an annealing furnace and kept for 2 h at 250 °C. Then the furnace was switched off and the glass sample was allowed to cool. The densities of the prepared glass system are reported in Ref [20].

3. Results and discussion

The LAC of the TeO₂-WO₃-ZnF₂ glass systems was determined by;

$$I = I_0 e^{-\mu x} = I_0 e^{-\mu_m t} \quad (1)$$

where **I** represent the attenuated ionizing photons and **I₀** represent the non-attenuated ionizing photons. **t** represents the thickness of the material (cm) and **μ** is the LAC (cm⁻¹) [18]. MAC is a term that refers to the ability of ionizing photons to penetrate a specific material.

$$\mu_m = \frac{\mu}{\rho} = \frac{1}{\rho t} \ln \left(\frac{I_0}{I} \right) = \sum_i w_i (\mu/\rho)_i \quad (2)$$

where **μ_m** is the MAC, **ρ** describes the density of the material (g/cm³), and **w_i** is the weight of the fractional **i** element [18]. In radiation shielding, the HVL is a critical parameter that helps determine the exact thickness of shielding materials needed to reduce the incident ionizing photon intensity by half. The HVL of a material is the thickness of matter at which the incoming radiation's intensity is decreased by half. The HVL values change with the thickness of a material. The HVL (cm) values can be calculated using equation (3):

$$\text{HVL} = (\ln 2 / \mu) \quad (3)$$

The TVL value, on the other hand, indicates the thickness of matter at which the incoming radiation's intensity is decreased by one tenth of the primary grade. (equation 4):

$$\text{TVL} = (\ln 10 / \mu) \quad (4)$$

The MFP values refer to the average distance a particle travels through the material before interacting with another particle. MFP is a crucial factor in radiation shielding [22]. Equation 5 can be used to calculate the MFP.:

$$\text{MFP} = (1/\mu)$$

Figure 1A shows the LAC of the prepared glass samples, as the energy of the photon increases the recorded values of the LAC decrease. When the samples were exposed to a photon energy of 0.015 MeV (low photon energy), the LAC reached its maximum value. In the lower energy region, TWZ3 has the highest LAC value of 376.45 cm⁻¹. However, as the energy of the photon increases the LAC values of TWZ1 also increase. The K-shell absorption edges for the prepared glass samples are represented by the notable humps in the curve at 0.04 MeV. Similar behaviors were recognized for the obtained MAC values as shown in figure 1B. The presence of photoelectric interactions can explain the observed degradation of LAC and MAC values while the samples were exposed to gamma photons of low energy between 0.015 and 0.03 MeV. When the samples were exposed to gamma photons of medium energy (0.04-4 MeV), the Compton scattering interaction gradually degraded the LAC and MAC values. The LAC and MAC values for high energy gamma photons (above 4 MeV) gradually raised as the interaction between gamma photons and the samples moved into the pair production domain.

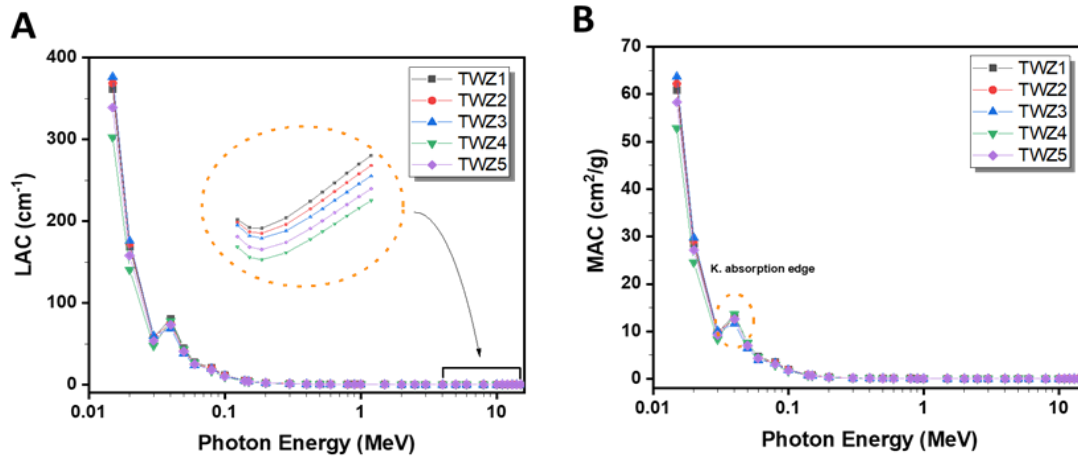


Fig. 1. The simulated reading for the linear attenuation coefficient (A) and the mass attenuation coefficient (B) for $\text{TeO}_2\text{-WO}_3\text{-ZnF}_2$ glass system.

HVL, MFP, and TVL have the lowest values at low energy gamma photons; however, as the photon energy increases, these values gradually rise until they reach their highest values around 6 MeV (see figure 2). These variances show that the calculated HVL, MFP, and TVL values have different photon energy interactions depending on the energy region. We obtained the HVL values for $\text{TeO}_2\text{-WO}_3\text{-ZnF}_2$ glass systems as shown in figure 2A. The HVL depends on the material density thus, low HVL values were obtained with denser shielding materials. Doping a chemical composition with a higher atomic number material can increase the density of certain chemical composition. Therefore, the TWZ1 glass sample with a density of 5.9456 g/cm^3 poses the lowest HVL value which can attenuate more ionizing radiation than the other glass samples, but TWZ3 sample has the lowest HVL value at low photon energy (0.015-0.03 MeV). The TVL was also observed in the same way as the HVL and shown in figure 2B. The MFP is one of the important parameters to evaluate the radiation shielding material. Lower MFP indicated superior radiation shielding properties for a particular material. Figure 2C shows the MFP values concerning the monoenergetic gamma photon energy for the prepared glass samples. Low MFP values recorded with denser materials make the TWZ1 have a better shielding characteristic compared with the other samples.

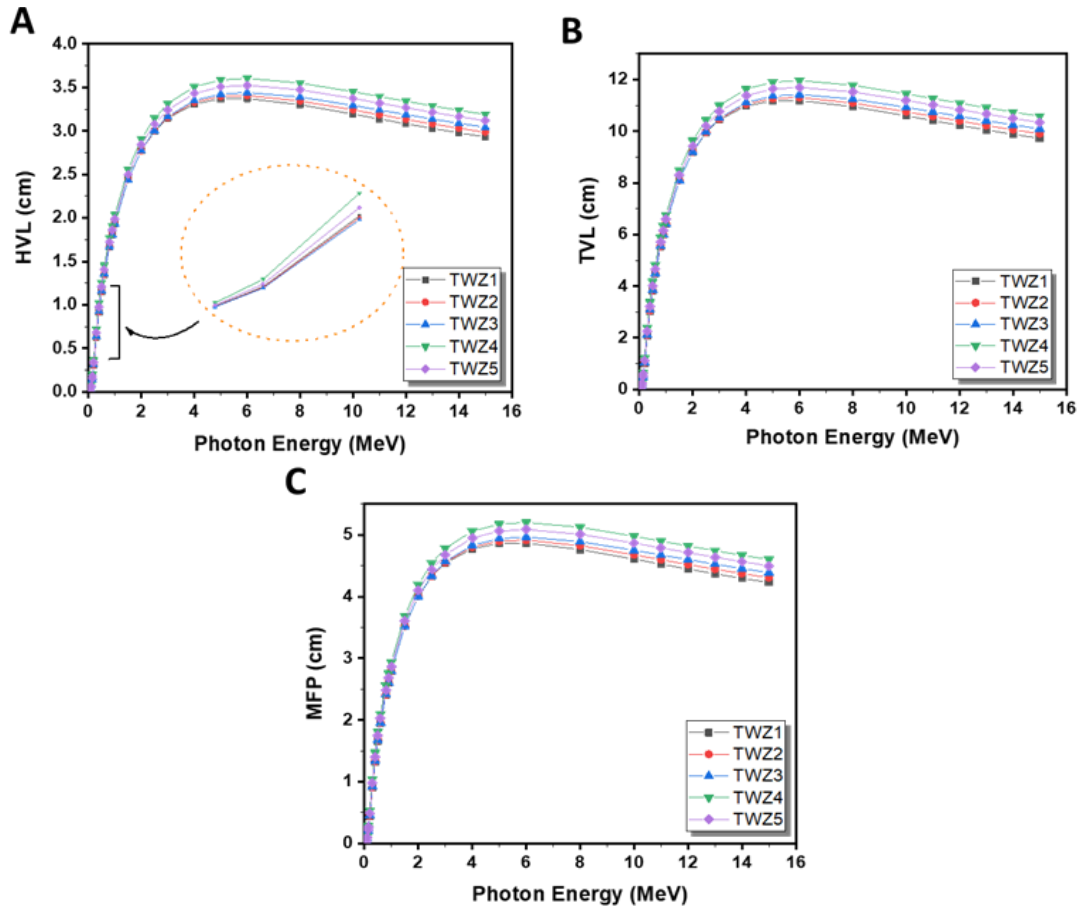


Fig. 2. The simulated reading for half value layer (A), tenth value layer (B), and mean free path (C) for $TeO_2-WO_3-ZnF_2$ glass system.

In terms of radiation shielding, both the effective atomic number (Z_{eff}) and the effective electron number (N_{eff}) are important considerations. Materials with a high atomic number and a high electron number can improve the efficacy of the radiation shielding material. Z_{eff} and N_{eff} should be considered when developing complex radiation-shielding materials. The Z_{eff} is mathematically defined as follows (equations 6):

$$Z_{eff} = \frac{\sigma_T}{\sigma_e} \quad (6)$$

where σ_t indicates the total atomic cross-section and σ_e indicates the total electronic cross-section. The N_{eff} indicates the number of electrons in a given mass unit. [18]. Additionally, N_{eff} is closely related to Z_{eff} , and can be determined by the following equation 7:

$$N_{eff} = \frac{N_A}{\sum_i f_i A_i} Z_{eff} \sum n_i = \frac{\mu_m}{\sigma_e} \quad (7)$$

where N_A represents the Avogadro number, f_i is the mol fraction of the i^{th} compound element in the radiation-shielding material, A_i represents the atomic weight, and $\sum n_i$ represents the total number of elements that are combined to form the proposed radiation shielding materials [18]. The total atomic cross-section (ACS) and total electronic cross-section (ECS) can be used to calculate the probability of photon interaction with the material. Both values can be measured using the SI unit $cm^2 g^{-1}$. Equations 8 and 9 are mathematical expressions for ACS and ECS:

$$ACS = \sigma_T = \frac{\mu}{\rho} = \frac{\sum_i f_i A_i}{N_i} \mu_m \quad (8)$$

$$\text{ECS} = \sigma_e = \left[\frac{1}{N_A} \right] \sum_i \left(\frac{f_i A_i}{Z_i} (\mu_m)_i \right) \quad (9)$$

where N_A indicates the Avogadro number, Z_i represents the atomic number, and A_i is the atomic weight [18].

Atomic and electronic numbers are used to describe the properties of a wide variety of materials. These are defined as the Z_{eff} and N_{eff} for a complex compound containing more than one element. Knowing the energy-dependent values for Z_{eff} and N_{eff} allows for an overall understanding of the material's behavior toward the incident ionizing radiation. Figures 3A and 3B show that the computed values of Z_{eff} and N_{eff} were the highest for the TWZ1 glass sample and the lowest for the TWZ4 glass sample. The Z_{eff} and N_{eff} values are largely affected by the incident photon energy. Photoelectric interactions induce a significant decrease in the Z_{eff} and N_{eff} values in the lower energy zone, while Compton scattering keeps them steady in the middle energy region. As the energy increases, the values progressively increase again owing to pair production. This link demonstrates how the photoelectric, Compton, and pair creation processes are all affected by the energy in the material. The N_{eff} value has a strong connection with electron cross-section (ECS) and MAC values, hence the N_{eff} results were calculated using the reported ECS and MAC values.

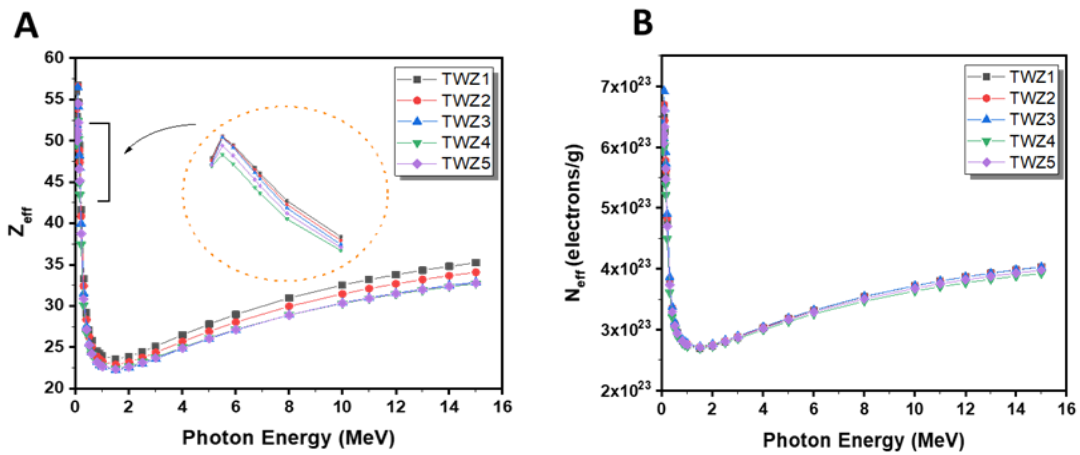


Fig. 3. The simulated reading for the effective atomic number (A) and the effective electron number (B) for $\text{TeO}_2\text{-WO}_3\text{-ZnF}_2$ glass system.

Figure 4A and 4B shows the simulated value for the ACS and ECS. For a certain radiation shielding material, the ACS and ECS values provide a precise possibility of radiation interaction per atom or electron in unit volume. Higher values of ACS and ECS mean that material has superior radiation shielding properties since it has a higher number of atoms or electrons per unit volume. In figure 4A, the TWZ1 sample has the highest ACS value which corresponded with the previously mentioned features as far as the obtained values for LAC, MAC, HVL, MFP, and TVL. In figure 4B, the TWZ3 glass sample has the highest ECS value in the low energy photon region, while the TWZ1 glass sample with the highest ECS value in the medium and high energy region.

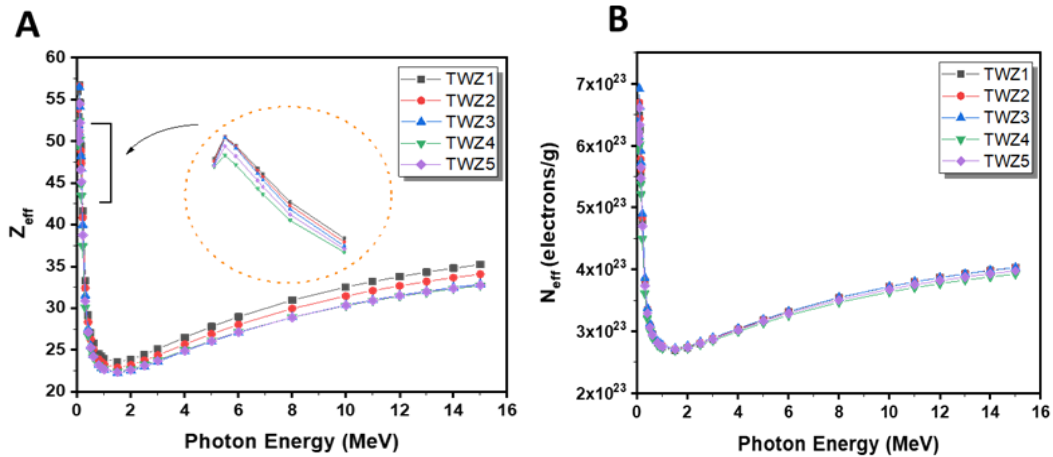


Fig. 4. The simulated reading for the atomic cross section (A) and the electronic cross section (B) for $\text{TeO}_2\text{-WO}_3\text{-ZnF}_2$ glass system.

The Raman spectra of $\text{ZnF}_2\text{-WO}_3\text{-TeO}_2$ glasses are shown in Fig. 5. The stretching vibrations of Te–O–Te links of TeO_4 trigonal bipyramids were allocated to a band in the glass spectrum at around 490cm^{-1} (tbp). Te–O stretching vibration of TeO_4 tbp units was attributed to the intense band at 710cm^{-1} [20, 38]. Furthermore, the spectra of the produced glasses revealed a substantial band at 800cm^{-1} according to TeO_3 units. Due to W–O stretchings in the WO_4 units, the spectra also revealed bands at 880cm^{-1} . The intensity of the bands due to WO_6 , TeO_{3+1} , TeO_3 phases structural units increases progressively when the concentration of WO_3 is increased, otherwise, the strength of bands due to TeO_4 and WO_4 structural units decreases. When WO_3 is incorporated into a TeO_2 glass network, W–O–W and Te–O–W connections occur with higher electronic polarizability leads to an increase in the connectivity of the glass network.

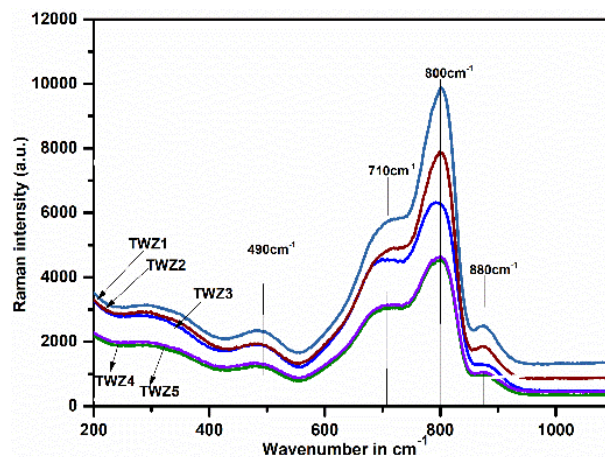


Fig. 5. Raman spectra of prepared glasses.

4. Conclusion

The LAC and MAC readings for the TWZ1 sample were highest thus better than the other samples. However, the TWZ3 sample with an LAC value of 376.45 cm^{-1} is better in the lower energy state. The TWZ1 glass sample with a density of 5.9456 g/cm^3 poses the lowest HVL but, the TWZ3 sample has the lowest HVL value at low photon energy (0.015-0.03 MeV). Furthermore, the computed values of Z_{eff} and N_{eff} were the highest for the TWZ1 glass sample and the lowest for the TWZ4 glass sample. Nevertheless, the TWZ1 sample obtained the highest ACS,

and ECS value in the medium and high energy region. However, the TWZ3 glass sample achieved the highest ECS value in the low-energy photon region. The glasses have a high concentration of W–O–W and Te–O–W linkage leads to improving the attenuation of radiation properties. This study demonstrates that the TeO₂-WO₃-ZnF₂ glass systems can be implemented for radiation protection purposes in a variety of applications at low energy.

Acknowledgments

The authors extend their appreciation to the Deanship of Scientific Research at King Khalid University (KKU) for funding this research project Number (R.G.P2/79/41).

References

- [1] Holmberg, O., Malone, J., Rehani, M., McLean, D., & Czarwinski, R., *European Journal of Radiology* **76**(1), 15 (2010); <https://doi.org/10.1016/j.ejrad.2010.06.033>
- [2] El-Qahtani, Z., M., Shaaban, H., E. R., Soraya, M., M., 2021. Attenuation characteristics of high-energy radiation on As-Se-Sn chalcogenide glassy alloy. *Chalcogenide Letters* ,18 (6),311 – 326 (2021).
- [3] Jakubowska, T., Długosz-Lisiecka, *Radiation Physics and Chemistry* **171**, 108688 (2020); <https://doi.org/10.1016/j.radphyschem.2020.108688>
- [4] Lakshminarayana, G., Baki, S. O., Kaky, K. M., Sayyed, M. I., Tekin, H. O., Lira, A., Mahdi, M. A.; *Journal of Non-Crystalline Solids* **471**, 222 (2017); <https://doi.org/10.1016/j.jnoncrysol.2017.06.001>
- [5] El-Mallawany, R., Sayyed, M. I., Dong, M. G., *Journal of Non-Crystalline Solids* **474**, 16 (2017); <https://doi.org/10.1016/j.jnoncrysol.2017.08.011>
- [6] Susoy, G., *Ceramics International* **46**(3), 3844 (2020); <https://doi.org/10.1016/j.ceramint.2019.10.108>
- [7] Sadetzki, S., Mandelzweig, L., *British journal of cancer* **100**(7), 1021 (2009); <https://doi.org/10.1038/sj.bjc.6604994>
- [8] Vano, E., *Radiation protection dosimetry* **147**(1-2), 3 (2011); <https://doi.org/10.1093/rpd/ncr265>
- [9] Mettler, F. A., *Journal of Radiological Protection* **32**(1), N9 (2012); <https://doi.org/10.1088/0952-4746/32/1/N9>
- [10] Singh, V. P., Badiger, N. M., Kaewkhao, J., *Journal of non-crystalline solids* **404**, 167 (2014); <https://doi.org/10.1016/j.jnoncrysol.2014.08.003>
- [11] Singh, K., Singh, S., Dhaliwal, A. S., & Singh, G., *Applied Radiation and Isotopes* **95**, 174 (2015); <https://doi.org/10.1016/j.apradiso.2014.10.022>
- [12] Schueler, B. A., *Techniques in vascular and interventional radiology* **13**(3), 167 (2010); <https://doi.org/10.1053/j.tvir.2010.03.005>
- [13] Li, Q., Wei, Q., Zheng, W., Zheng, Y., Okosi, N., Wang, Z., Su, M., *ACS applied materials & interfaces* **10**(41), 35510 (2018); <https://doi.org/10.1021/acsami.8b10600>
- [14] Nagaraja, N., Manjunatha, H. C., Seenappa, L., Sridhar, K. N., Ramalingam, H. B., *Radiation Physics and Chemistry* **171**, 108723 (2020); <https://doi.org/10.1016/j.radphyschem.2020.108723>
- [15] Akman, F., Khattari, Z. Y., Kaçal, M. R., Sayyed, M. I., Afaneh, F., *Radiation Physics and Chemistry* **160**, 9 (2019); <https://doi.org/10.1016/j.radphyschem.2019.03.001>
- [16] Şakar, E., Özpolat, Ö. F., Alim, B., Sayyed, M. I., & Kurudirek, M., *Radiation Physics and Chemistry* **166**, 108496 (2020); <https://doi.org/10.1016/j.radphyschem.2019.108496>
- [17] Waly, E. S. A., Fusco, M. A., & Bourham, M. A., *Annals of Nuclear Energy* **96**, 26 (2016); <https://doi.org/10.1016/j.anucene.2016.05.028>
- [18] AbouDeif, Y. M., Alqahtani, M. S., Massoud, E. E., Yaha, I. S., Yousef, E., *Journal of Instrumentation* **15**(08), P08005 (2020); <https://doi.org/10.1088/1748-0221/15/08/P08005>

- [19] Sayyed, M. I., Laariedh, F., Kumr, A., & Al-Buriahi, M. S., *Applied Physics A* **126**(1), 1 (2020); <https://doi.org/10.1007/s00339-019-3182-8>
- [20] Yousef, E., Hotzel, M., & Rüssel, C., *Journal of non-crystalline solids* **342**(1-3), 82 (2004); <https://doi.org/10.1016/j.jnoncrysol.2004.07.003>
- [21] Othman, H., A., Alqahtani, M. M., Reben, M., Yousef, El S. (2020) Raman Gain and Structural of Tellurite-Phosphate Glasses with Different Modifiers doping with Er₂O₃, *Chalcogenide Letters*, 17(4), 207-215 (2020)..
- [22] Kamislioglu, M., Guclu, E. A., Tekin, H. O., *Applied Physics A* **126**(2), 1 (2020); <https://doi.org/10.1007/s00339-020-3284-3>
- [23] El-Mallawany, R., Abd El-Moneim, A., *Physica Status Solidi A* **166**(2), 829 (1998); [https://doi.org/10.1002/\(SICI\)1521-396X\(199804\)166:2<829::AID-PSSA829>3.0.CO;2-Y](https://doi.org/10.1002/(SICI)1521-396X(199804)166:2<829::AID-PSSA829>3.0.CO;2-Y)
- [24] Alomairy, S., Al-Buriahi, M. S., Wahab, E. A., Sriwunkum, C., Shaaban, K., *Ceramics International*, 47(12), 17322 (2021); <https://doi.org/10.1016/j.ceramint.2021.03.045>
- [25] Naik, P. S. R., Kumar, M. K., Babu, Y. C. R., & Kumar, A. S., *Indian Journal of Physics* **87**(8), 757 (2013); <https://doi.org/10.1007/s12648-013-0284-6>
- [26] Chen, Q., *Journal of Non-Crystalline Solids* **522**, 119584 (2019); <https://doi.org/10.1016/j.jnoncrysol.2019.119584>
- [27] Stalin, S., Gaikwad, D. K., Al-Buriahi, M. S., Srinivasu, C., Ahmed, S. A., Tekin, H. O., Rahman, S., *Ceramics International*, 47(4), 5286 (2021); <https://doi.org/10.1016/j.ceramint.2020.10.109>
- [28] ElBatal, H. A., Abdelghany, A. M., ElBatal, F. H., EzzElDin, F. M., *Materials Chemistry and Physics* **134**(1), 542 (2012); <https://doi.org/10.1016/j.matchemphys.2012.03.032>
- [29] Kaur, A., Khanna, A., Sathe, V. G., Gonzalez, F., Ortiz, B., *Phase Transitions* **86**(6), 598 (2013); <https://doi.org/10.1080/01411594.2012.727998>
- [30] Tanaka, K., Narazaki, A., Hirao, K., *Optics Letters* **25**(4), 251 (2000); <https://doi.org/10.1364/OL.25.000251>
- [31] Kilic, G., Issever, U. G., Ilik, E., *Journal of Non-Crystalline Solids* **527**, 119747 (2020); <https://doi.org/10.1016/j.jnoncrysol.2019.119747>
- [32] Patil, S. D., Jali, V. M., Anavekar, R. V., *Bulletin of Materials Science* **31**(4), 631 (2008); <https://doi.org/10.1007/s12034-008-0100-7>
- [33] Sidebottom, D. L., Green, P. F., & Brow, R. K., *Journal of non-crystalline solids* **222**, 354 (1997); [https://doi.org/10.1016/S0022-3093\(97\)00406-7](https://doi.org/10.1016/S0022-3093(97)00406-7)
- [34] Yuliantini, L., Kaewnuam, E., Hidayat, R., Djamal, M., Boonin, K., Yasaka, P., Kaewkhao, J., *Optical Materials* **85**, 382 (2018); <https://doi.org/10.1016/j.optmat.2018.09.007>
- [35] Zhang, W., Lin, J., Sun, G., Jia, Y., Zhao, J., Ye, S., Rong, L., *Optical Materials* **36**(6), 1013 (2014); <https://doi.org/10.1016/j.optmat.2014.01.003>
- [36] Chillce, E. F., Mazali, I. O., Alves, O. L., Barbosa, L. C., *Optical Materials* **33**(3), 389 (2011); <https://doi.org/10.1016/j.optmat.2010.09.027>
- [37] Miguel, A., Morea, R., Gonzalo, J., Arriandiaga, M. A., Fernández, J., Balda, R., *Journal of Luminescence* **140**, 38 (2013); <https://doi.org/10.1016/j.jlumin.2013.02.059>
- [38] El Sayed, S. Y., *Journal of Physics D: Applied Physics* **38**(21), 3970 (2005); <https://doi.org/10.1088/0022-3727/38/21/022>
- [39] Hussein, K. I., Alqahtani, M. S., Algarni, H., Zahran, H., Yaha, I. S., Grelowska, I., Yousef, E. S., *Journal of Instrumentation* **16**(07), T07004 (2021); <https://doi.org/10.1088/1748-0221/16/07/T07004>
- [40] Gerward, L., Guilbert, N., Jensen, K. B., Leving, H., *Radiation physics and chemistry* **71**(3-4), 653 (2004); <https://doi.org/10.1016/j.radphyschem.2004.04.040>